BCSJ Award Article

Surface Modification of TaON with Monoclinic ZrO_2 to Produce a Composite Photocatalyst with Enhanced Hydrogen Evolution Activity under Visible Light

Kazuhiko Maeda,[1,3] Hiroaki Terashima,[2] Kentaro Kase,[2] Masanobu Higashi,[1] Masashi Tabata,[1] and Kazunari Domen*[1]

[1]Department of Chemical System Engineering, The University of Tokyo, 7-3-1 Hongo, Bunkyo-ku, Tokyo 113-8656

[2]Catalytic Chemistry Division, Chemical Resources Laboratory, Tokyo Institute of Technology, 4259 Nagatsuta, Midori-ku, Yokohama 226-8503

[3]Research Fellow of the Japan Society for the Promotion of Science (JSPS)

Received March 10, 2008; E-mail: domen@chemsys.t.u-tokyo.ac.jp

A composite material consisting of tantalum oxynitride (TaON) and monoclinic zirconium oxide (*m*-ZrO_2) is prepared by a surface modification method as a photocatalyst with enhanced activity for H_2 evolution from water under visible light ($\lambda > 420$ nm). The composite is prepared by loading particulate Ta_2O_5 with nanoparticulate *m*-ZrO_2 followed by nitridation at 1123 K for 15 h under NH_3 flow. The activity of the *m*-ZrO_2/TaON composite for H_2 evolution from aqueous methanol solution is higher than that of either *m*-ZrO_2 or TaON when loaded with nanoparticulate ruthenium as a H_2 evolution site. The highest activity is obtained using a composite prepared with a Zr/Ta molar ratio of 0.1. The optimized material also provides elevated activity when used as an H_2 evolution photocatalyst in Z-scheme overall water splitting in combination with Pt-loaded WO_3 as an O_2 evolution photocatalyst and an IO_3^-/I^- shuttle redox mediator. The improvement in activity is attributed to the suppression of surface defect formation by inhibiting tantalum reduction during nitridation.

Tantalum oxynitride (TaON)[1] has been studied extensively as a visible-light-responsive photocatalyst[2–4] and photoelectrode.[5,6] In particular, this material is a promising candidate as an overall water-splitting photocatalyst to produce clean hydrogen fuel, due to its suitable band-edge position[7] and stability in aqueous media[8] and under photoirradiation.[2a] However, a major drawback of TaON as a photocatalyst is its low activity for water reduction (i.e. H_2 evolution),[2] which can be attributed in part to the inherently high defect density of TaON and the lack of a suitable modification method to improve its reduction behavior.[9] It is therefore important to develop a new modification and/or preparation method that enhances the H_2 evolution activity of TaON.

TaON can be obtained by heating Ta_2O_5 powder under flowing NH_3 at high temperatures and has a baddelyite-type structure,[10] as illustrated schematically in Figure 1. In most cases, defects exist on both the surface and in the bulk of solid photocatalysts, suppressing activity by acting as recombination centers between photogenerated electrons and holes. To realize a highly active solid photocatalyst, it is thus indispensable to eliminate defects in the material. The general strategy adopted to date to reduce defect density has been to increase the crystallinity of the material by refining the preparation parameters.[11–15] However, it is difficult to control the crystallinity of TaON by adjustment of preparation parameter alone because TaON is an intermediate phase between Ta_2O_5 and Ta_3N_5.[2a,16] Although the calcination of solid photocatalysts after preparation has been demonstrated to be an effective approach for re-

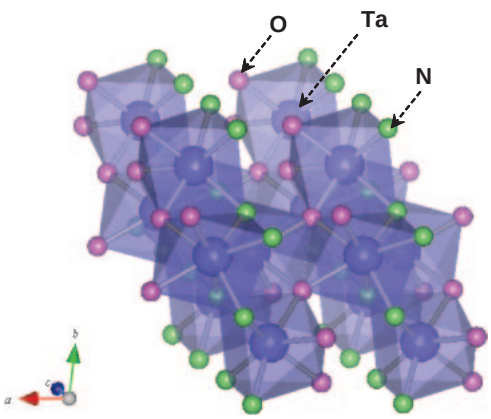

Figure 1. Crystal structure of TaON.

Published on the web August 11, 2008; doi:10.1246/bcsj.81.927

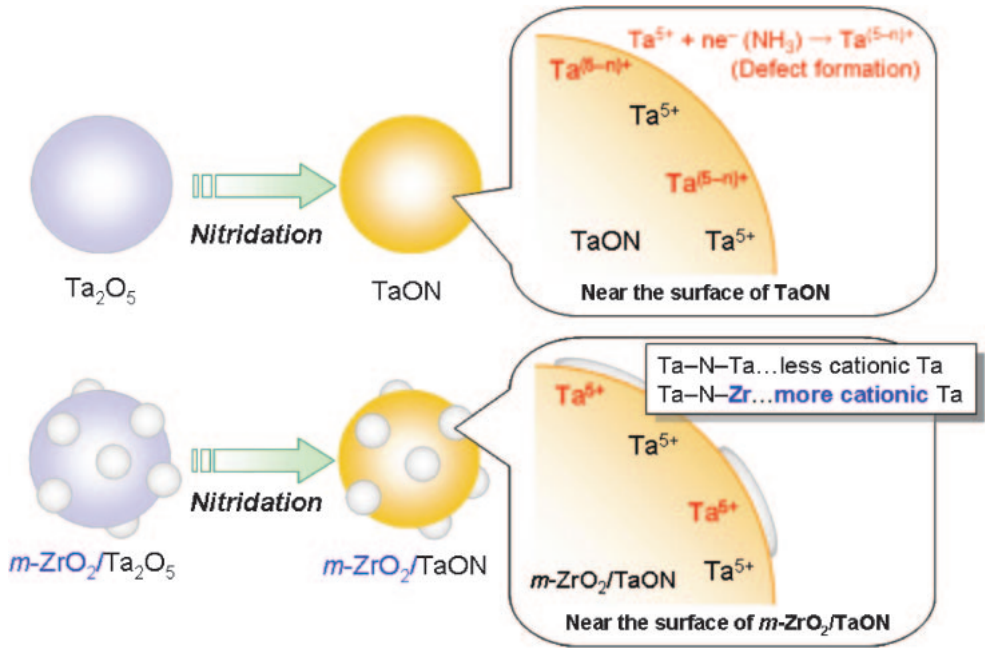

Scheme 1. Nitridation of m-ZrO_2/Ta_2O_5 composite to produce m-ZrO_2/TaON while suppressing the production of reduced tantalum species (defect sites) near the surface of the material.

ducing the density of defects,[17,18] such post-calcination appears to be disadvantageous for TaON due to its low thermal stability. In fact, post-calcination of TaON under O_2 or N_2 results in a decrease in activity.[6] The elimination of defects in TaON therefore remains a challenge.

Zirconia (ZrO_2) and related compounds are interesting materials that have applications as electrolytes in solid oxide fuel cells,[19] as high-temperature structural ceramics,[20] and in catalysis[21] and photocatalysis.[22–26] ZrO_2 has three polymorphs: monoclinic, tetragonal, and cubic. In general, the monoclinic form is the stable phase at room temperature. At elevated temperatures (>1443 K), the tetragonal phase becomes stable, followed by the cubic phase at even higher temperatures (>2643 K). Monoclinic ZrO_2 (m-ZrO_2) has a band gap of 5.0 eV, and display high photocatalytic activity for overall water splitting when irradiated at ultraviolet (UV) wavelengths ($\lambda > 200$ nm).[23] It has been reported that m-ZrO_2 and TaON can form a solid solution ($Zr_xTa_{1-x}O_{1+x}N_{1-x}$) with a baddeleyite structure over the compositional range of $0 < x < 0.28$, and the resultant compound has been found to have a larger band gap energy than TaON.[27,28]

In the present study, we show a new strategy to reduce surface defects on TaON using ZrO_2 as a "protector" through a surface modification technique. Specifically, m-ZrO_2 nanoparticles are dispersed on the surface of Ta_2O_5 precursor before nitridation, thereby protecting Ta^{5+} cations in the TaON surface from being reduced by H_2 (derived from disassociation of NH_3 at high temperatures) during nitridation. As has been observed for other (oxy)nitrides such as $LaTiO_2N$[29] and $TiN_xO_yF_z$,[30] the reduction of Ta^{5+} cations in TaON during nitridation generates reduced tantalum species, which can act as recombination centers between photogenerated electrons and holes. On the other hand, when m-ZrO_2 is loaded on the surface of Ta_2O_5, tantalum cations at the interface between Ta_2O_5 (and/or TaON) and the loaded m-ZrO_2 are expected to interact with m-ZrO_2 and thereby become more cationic. As a result, the formation of reduced tantalum species on the TaON surface is considered to be suppressed by prior loading with nanoparticulate m-ZrO_2. The fact that the temperature required for nitridation of ZrO_2 is higher than that of TaON[31] is also favorable for taking this scenario. The above-mentioned strategy is illustrated in Scheme 1. This paper reports on characterization and visible-light photocatalytic activity of the thus-obtained composite material of m-ZrO_2 and TaON. The composite material becomes an active catalyst not only for H_2 evolution from an aqueous methanol solution but also for overall water splitting in Z-scheme under visible-light irradiation ($\lambda >$ 420 nm), with higher activities than TaON alone.

Experimental

Preparation of Catalysts. Ta_2O_5 loaded with nanoparticulate m-ZrO_2 (m-ZrO_2/Ta_2O_5) was prepared with a range of Zr/Ta molar ratios as precursors for m-ZrO_2/TaON composites by the following solid-state reaction. $ZrO(NO_3)_2 \cdot 2H_2O$ (99%; Kanto Chemicals) and Ta_2O_5 (99.9%; High Purity Chemicals) powders were mixed well using a small amount of methanol, and then dried in an oven at 343 K for 1 h. The resulting powder was subsequently heated in air at 1073 K for 2 h using an Al_2O_3 crucible. The m-ZrO_2/TaON composite material was prepared by heating the as-prepared m-ZrO_2/Ta_2O_5 powder to 1123 K at 10 K min^{-1} under a flow of NH_3 (20 mL mL^{-1}). The material was heated at that temperature for 15 h. The sample was then cooled to room temperature under NH_3 flow.

For comparison, a solid solution of m-ZrO_2 and TaON (Zr/Ta = 0.1 by mole) was also prepared according to previously reported method.[28] A mixed-oxide of zirconium and tantalum as the precursor for the solid solution was prepared by the polymerized complex method reported by Kakihana et al.,[32] as follows. Initially, 7.623 g of $TaCl_5$ (99.99%; High Purity Chemicals) and 0.686 g of $ZrOCl_2 \cdot 6H_2O$ (98%; High Purity Chemicals) were dissolved in 150 mL of methanol (99.8%; Kanto Chemicals). After

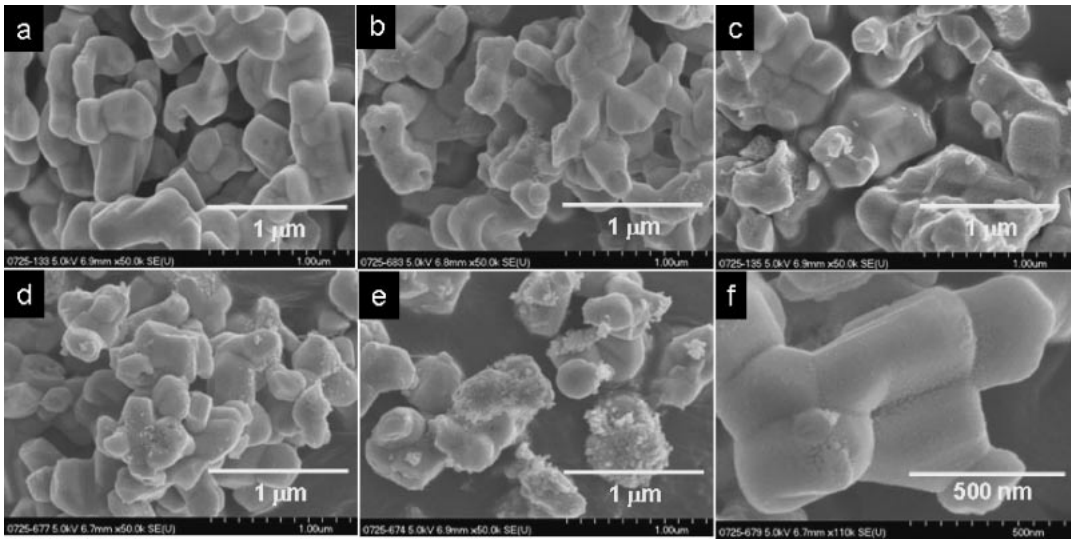

Figure 2. SEM images of samples obtained by solid-state reaction between $ZrO(NO_3)_2 \cdot 2H_2O$ and Ta_2O_5 in air at 1073 K for 2 h with Zr/Ta molar ratios of (a) 0 (Ta_2O_5), (b) 0.05, (c) 0.1, (d) 0.15, and (e) 0.2. (f) High-resolution image of (b).

complete dissolution, 30 g of ethylene glycol (EG) (99.5%; Kanto Chemicals) and 22.8 g of anhydrous citric acid (CA) (98.0%; Wako Pure Chemicals) were added to the solution. The solution was then heated overnight at ca. 400 K to promote esterification between EG and CA, yielding a glassy resin. The resin was then calcined at ca. 623 K in a mantle heater to complete decomposition. Finally, the resulting black powder was calcined on an Al_2O_3 plate at 923 K for 2 h in air, and then calcined a second time at 1073 K for 2 h. The as-prepared material was nitrided in the same manner as the composite material above. The product thus obtained is referred to a *m*-ZrO_2–TaON. For use as references in characterization, *m*-ZrO_2 powder (99%) was used as purchased from Kanto Chemicals, and Ta_3N_5 was prepared according to the method reported in a previous paper.[2b]

Nanoparticulate ruthenium and platinum were employed as cocatalysts to enhance the photocatalytic activity for H_2 evolution. Ruthenium-loaded *m*-ZrO_2/TaON was prepared by an in situ photodeposition method according to the method reported in previous papers.[2c,2d] The rate of ruthenium loading was 0.05 wt % (metallic content). Modification of *m*-ZrO_2/TaON with nanoparticulate platinum was carried out by an impregnation method from an aqueous solution containing $H_2[PtCl_6]$, followed by heating under an H_2 gas stream at 473 K for 1 h. Platinum-loaded WO_3 was prepared as an O_2 evolution photocatalyst for Z-scheme overall water splitting[4,33,34] by immersing WO_3 (99.99%; High Purity Chemicals) in aqueous $H_2[PtCl_6]$ solution, followed by calcination in air at 823 K for 0.5 h. The rate of platinum loading was 0.5 wt % (metallic content) in both cases.

Characterization of Catalysts. The prepared samples were studied by powder X-ray diffraction (XRD; RINT-UltimaIII, Rigaku; Cu Kα), scanning electron microscopy (SEM; S-4700, Hitachi), energy dispersive X-ray spectroscopy (EDX; Emax-7000, Horiba), X-ray absorption fine structure (XAFS) spectroscopy, X-ray photoelectron spectroscopy (XPS; JPS-9000, JEOL), and UV–visible diffuse reflectance spectroscopy (DRS; V-560, JASCO). XAFS measurements were carried out at the BL9A beamline of the Photon Factory (High Energy Accelerator Research Organization, Tsukuba, Japan) using a ring energy of 2.5 GeV and stored current from 450–300 mA (Proposal No. 2007G624). The X-ray absorption spectra were measured in transmission mode at room temperature using an Si(111) two-crystal monochromator. Data reduction was performed using the REX2000 program (Rigaku). The photon energies in X-ray absorption near-edge structure (XANES) spectra were corrected in reference to copper foil (8980.3 eV) for each sample. The binding energies determined by XPS were corrected in reference to the C 1s peak (284.6 eV) for each sample. The Brunauer–Emmett–Teller (BET) surface area was measured using a BELSORP-mini instrument (BEL Japan) at liquid nitrogen temperature.

Photocatalytic Reactions. Reactions were carried out in a Pyrex top irradiation-type reaction vessel connected to a glass closed gas circulation system. Photoreduction of H^+ to H_2 and photooxidation of H_2O to O_2 were performed separately in aqueous solutions containing methanol or silver nitrate as sacrificial reagents, respectively. For water photoreduction, 0.4 g of the catalyst was dispersed in the aqueous methanol solution (80 vol %, 100 mL) containing an appropriate amount of $(NH_4)_2[RuCl_6]$. For water photooxidation, 0.4 g of the catalyst and 0.2 g of La_2O_3 powder were dispersed in the aqueous silver nitrate solution (10 mM, 100 mL). La_2O_3 buffers the pH of the reactant solution to pH 8–9 during the reaction.[2a,2b] For Z-scheme overall water splitting,[4] 0.1–0.2 g of Pt-loaded *m*-ZrO_2/TaON as an H_2 evolution catalyst and 0.2 g of Pt-loaded WO_3 as an O_2 evolution catalyst were suspended in an aqueous NaI solution (1 mM, 100 mL). The reactant solution was then evacuated several times to remove air completely prior to irradiation under a 300 W xenon lamp fitted with a cutoff filter and a water filter ($\lambda > 420$ nm). The temperature of the reactant solution was maintained at room temperature by a flow of cooling water during the reaction. The evolved gases were analyzed by gas chromatography.

Results and Discussion

Characterization of Oxide Precursors for Nitridation. Figure 2 shows SEM images of the samples obtained by solid-state reaction between $ZrO(NO_3)_2 \cdot 2H_2O$ and Ta_2O_5 in air at 1073 K for 2 h. In the calcined Ta_2O_5 powder, primary particles of 300–500 nm in size are sintered together to form larger secondary particles of 500–800 nm in size (Figure 2a). The solid-state reaction between $ZrO(NO_3)_2 \cdot 2H_2O$ and Ta_2O_5 re-

sulted in the appearance of nanoparticles on the Ta_2O_5 surface. All samples containing zirconium species exhibited a relatively uniform distribution of fine particles (<10 nm), which were confirmed by EDX analysis to be zirconium species in all cases (Figure 2f). Aggregates of the fine zirconium species were occasionally observed (30–80 nm). The size of zirconium species and the degree of aggregation increased with the Zr/Ta molar ratio without affecting the particle size of Ta_2O_5.

XRD analyses showed that all prepared samples exhibit the same diffraction patterns as Ta_2O_5 with no noticeable change in peak position (see Supporting Information, Figure S1). No diffraction peaks attributable to zirconium species or Zr–Ta-mixed oxide are apparent, regardless of the Zr/Ta molar ratio. It has been reported that $ZrO(NO_3)_2$ decomposes in air at temperatures above 973 K to give *m*-ZrO_2,[35] and it was confirmed by the present XRD analyses that calcination of $ZrO(NO_3)_2 \cdot 2H_2O$ in air at 1073 K for 2 h results in the production of *m*-ZrO_2 (line g, Figure S1). The zirconium species loaded on Ta_2O_5 are therefore considered to be the monoclinic form, although the crystalline phase could not be observed due to the small particle size with high dispersion (Figure 2). Homs et al. reported the development of a Zr–Ta-mixed oxide ($TaZr_{2.75}O_8$) upon calcination of solids prepared by a sol–gel method using zirconium propoxide and tantalum ethoxide.[36] Under the present preparation conditions, however, no such mixed oxide was formed, probably due to heterogeneity of the starting material (mixture of $ZrO(NO_3)_2 \cdot 2H_2O$ and Ta_2O_5) and/or relatively low calcination temperature (1073 K).

Structural Properties of Nitridation Products. Figure 3 shows XRD patterns of *m*-ZrO_2/Ta_2O_5 composite materials with various Zr/Ta molar ratios after nitridation. Ta_2O_5, Ta_3N_5, *m*-ZrO_2–TaON solid solution, and *m*-ZrO_2 data are shown for comparison. The samples prepared with Zr/Ta molar ratios of less than 0.1 exhibit single-phase diffraction patterns indicative of a monoclinic baddelyite structure similar to TaON and *m*-ZrO_2. As the Zr/Ta molar ratio becomes larger than 0.15, however, small peaks assignable to *m*-ZrO_2 appear (lines e and f). No peaks attributable to Ta_2O_5, Ta_3N_5, or zirconium (oxy)nitride were observed for any of the prepared samples. Miyake et al. reported that the nitridation of amorphous zirconium oxide at 1173 K under NH_3 flow results in the formation of zirconium oxynitride with various crystal phases depending on the nitridation time.[31] In the present study, however, the nitridation temperature was lower than that reported for the synthesis of zirconium oxynitride, and it was confirmed that the nitridation of *m*-ZrO_2 at 1123 K for 15 h under NH_3 flow does not produce zirconium oxynitrides (data not shown). The positions of the diffraction peaks of the reference solid solution (*m*-ZrO_2–TaON) were shifted slightly to lower 2θ angles (line h) to lie between those of *m*-ZrO_2 (line i) and TaON (line b). This peak shift is reasonable considering the relatively large *a* and *b* lattice constants of *m*-ZrO_2 ($a = 5.3129$ Å, $b = 5.2125$ Å, $c = 5.1471$ Å)[37] compared to TaON ($a = 4.9494$ Å, $b = 5.0166$ Å, $c = 5.1642$ Å).[10] This peak shift confirms the production of a solid solution of *m*-ZrO_2 and TaON by the present preparation method, as reported previously.[27,28] No shifts in the diffraction peak positions were observed for any of the samples prepared using the *m*-ZrO_2/Ta_2O_5 composite material, regardless of the Zr/Ta molar ratio,

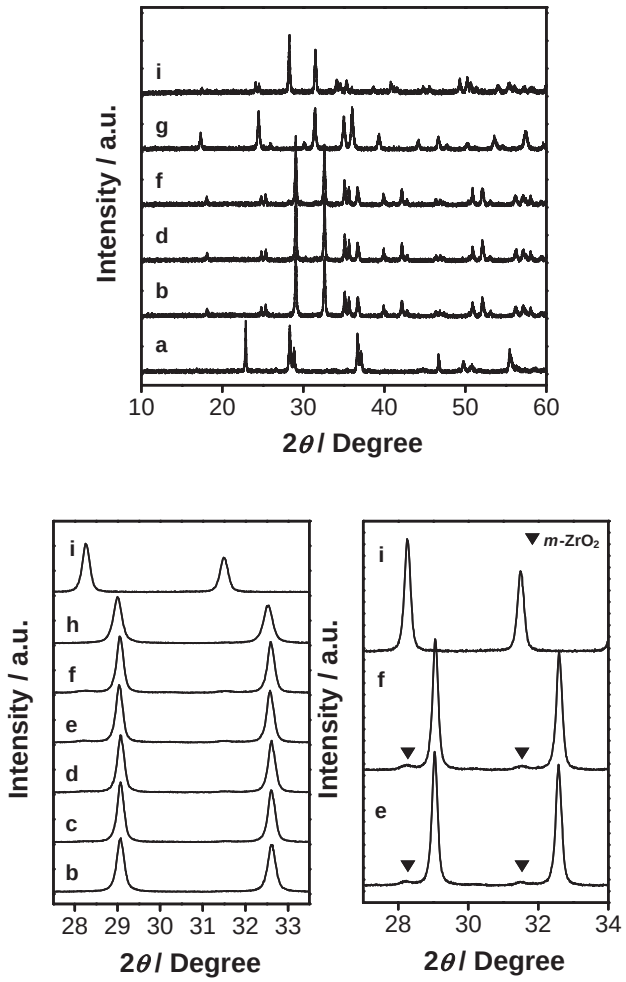

Figure 3. XRD patterns of samples obtained by nitriding *m*-ZrO_2/Ta_2O_5 with Zr/Ta molar ratios of (b) 0, (c) 0.05, (d) 0.1, (e) 0.15, and (f) 0.2 at 1123 K for 15 h under NH_3 flow. Data for (a) Ta_2O_5, (g) Ta_3N_5, (h) *m*-ZrO_2–TaON solid solution, and (i) *m*-ZrO_2 are shown for reference.

indicating that the formation of a solid solution between *m*-ZrO_2 and TaON did not take place.

The local structure of the prepared samples was studied by XAFS. The XANES spectra for all prepared samples are identical, but differ clearly from those for the Ta_2O_5 and Ta_3N_5 references (see Supporting Information, Figure S2). This result indicates that the local structure of the samples is very similar to TaON, regardless of the Zr/Ta molar ratio employed in preparation. Figure 4 shows the Fourier transforms (FTs) of the k^3-weighted Ta–L_{III} edge EXAFS spectra for TaON and the sample prepared with a Zr/Ta ratio of 0.1. The data for the *m*-ZrO_2–TaON solid solution is also shown for comparison. The peak at ca. 1.8 Å in the spectra is due to electron backscattering by neighboring oxygen and nitrogen atoms, while that at ca. 3.2 Å is ascribed to metal atoms located at a longer distance than oxygen and nitrogen atoms. The peak at ca. 3.8 Å is assignable to the third shell configuration derived from oxygen and nitrogen atoms. As can be seen, the FTs of the EXAFS spectra are essentially identical for all samples. However, comparison of the peak assigned to the second shell

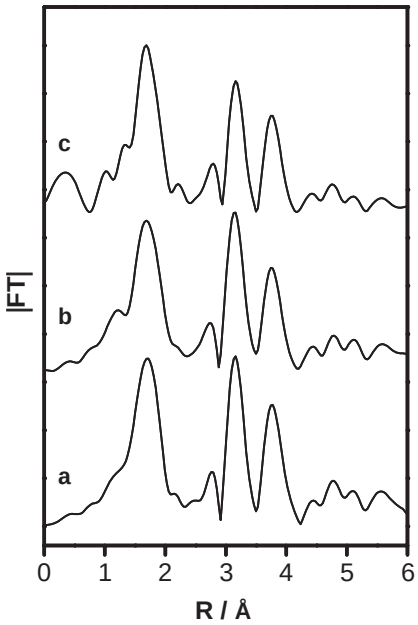

Figure 4. Fourier transforms of k^3-weighted Ta–L_{III} edge EXAFS spectra for samples obtained by nitriding *m*-ZrO_2/Ta_2O_5 with Zr/Ta molar ratios of (a) 0 and (b) 0.1 at 1123 K for 15 h under NH_3 flow. (c) Spectrum for *m*-ZrO_2–TaON solid solution (shown for reference).

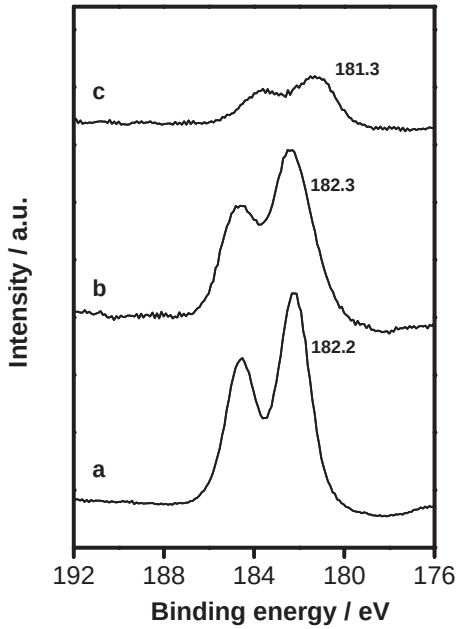

Figure 5. XPS spectra for Zr 3d in (a) *m*-ZrO_2, (b) the sample prepared with Zr/Ta ratio of 0.1, and (c) *m*-ZrO_2–TaON solid solution.

with that of the first shell suggests that the second shell configuration in the solid-solution sample (spectrum c) is weaker than those indicated in other spectra. When *m*-ZrO_2 and TaON form a solid solution, electron backscattering derived from the second shell configuration should become weaker due to the difference in atomic number between tantalum (73) and zirconium (40). The relative weakness of the peak due to the second shell configuration in the solid solution sample compared to that for TaON therefore confirms the formation of a solid solution of *m*-ZrO_2 and TaON, consistent with the XRD analysis (Figure 3). The sample with Zr/Ta = 0.1, on the other hand, does not exhibit any change in the second shell peak, indicating that the incorporation of *m*-ZrO_2 into the TaON lattice is negligible in that sample. This result is also in good agreement with the XRD results (Figure 3).

The atomic composition and the surface valence states of zirconium and tantalum in the prepared samples were investigated by XPS. Figure 5 shows the XPS spectrum for Zr 3d in the sample prepared with a Zr/Ta ratio of 0.1. The data for *m*-ZrO_2 and the *m*-ZrO_2–TaON solid solution are shown for comparison. The Zr $3d_{5/2}$ photoelectron signal for *m*-ZrO_2 appears at 182.2 eV (spectrum a), in good agreement with the reported values (182.1 eV).[38] The sample displays a photoelectron signal at the same binding energy as *m*-ZrO_2 (spectrum b). However, the Zr $3d_{5/2}$ peak for the *m*-ZrO_2–TaON solid solution appears at 181.3 eV (spectrum c), that is, at lower binding energy than for *m*-ZrO_2 and the *m*-ZrO_2/TaON sample. This shift in binding energy indicates that the zirconium species in the solid solution are less cationic than those in *m*-ZrO_2, which is attributable to the presence of nitrogen in the solid solution. It therefore appears that a Zr–N bond is formed in the solid solution. This suggestion is reasonable because each constituent element of the solid solution is atomically mixed with the others, as indicated by the XRD and XAFS measurements (Figures 3 and 4). Such a shift in binding energy due to a difference in bond polarity has also been observed for Ta_2O_5, TaON, and Ta_3N_5.[7,8] However, the Zr $3d_{5/2}$ peak for the present sample is not shifted with the respect to that for *m*-ZrO_2, indicating that the interaction between zirconium species and nitrogen species is not sufficiently strong to cause a peak shift, and that the valence state of zirconium species on the surface is close to that of *m*-ZrO_2.

The XPS spectrum for Ta 4f in the same sample is shown in Figure 6. The data for Ta_2O_5, the *m*-ZrO_2–TaON solid solution, and TaON (Zr/Ta = 0) are shown for comparison. As reported previously, TaON produces a photoelectron signal at lower binding energy (spectrum d) than Ta_2O_5 (spectrum a), which can be explained in terms of the difference in bond polarities of Ta–O and Ta–N as mentioned above; that is, the Ta–N bond is more covalent than the Ta–O bond.[7,8] TaON consists of TaO_3N_4 heptahedra in which oxygen and nitrogen atoms are corner- and edge-shared, respectively (Figure 1), with Ta–N bonds in the crystal.[10] The Ta $4f_{7/2}$ peaks for the present sample (spectrum b) and the *m*-ZrO_2–TaON solid solution (spectrum c) appear at almost the same position as that for the TaON reference. As the interaction between tantalum and oxygen atoms in TaON becomes stronger, the Ta $4f_{7/2}$ peak should shift to higher binding energies.[7,8] However, it appears that the interaction between oxygen and tantalum atoms in both the present sample and the solid solution is too weak to shift the XPS peak compared to that for TaON.

Table 1 lists the surface atomic compositions for several samples, as estimated from the areas of the corresponding XPS peaks. The Zr/Ta surface atomic ratio in the sample prepared with Zr/Ta = 0.1 (Entry 3) is larger than that in the solid solution (Entry 2). As both materials should contain zirconium and tantalum at the same ratio (Zr/Ta = 0.1) on average,

Table 1. Surface Atomic Ratios of TaON, *m*-ZrO_2–TaON Solid Solution, and *m*-ZrO_2/TaON Composite

Entry	Sample	Zr/Ta atomic ratio in sample	Surface atomic ratio[a)]		
			Zr/Ta	O/Ta[b)]	N/Ta
1	TaON	0	—	1.92	0.84
2	*m*-ZrO_2–TaON solid solution	0.1	0.17	1.70	0.82
3	*m*-ZrO_2/TaON composite	0.1	0.63	2.58	0.78
4	*m*-ZrO_2/TaON composite	0.2	1.01	3.35	0.84

a) Estimated from corresponding XPS peak areas. b) Estimated from entire peak area of O 1s and Ta 4f.

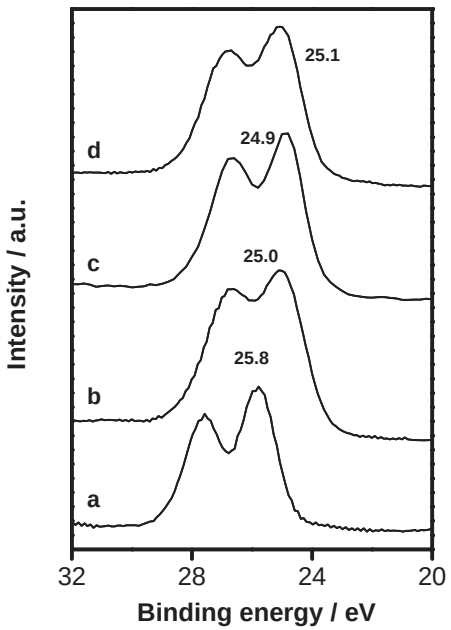

Figure 6. XPS spectra for Ta 4f in (a) Ta_2O_5, (b) the sample prepared with Zr/Ta ratio of 0.1, (c) *m*-ZrO_2–TaON solid solution, and (d) TaON (the sample prepared with Zr/Ta ratio of 0).

the difference in the Zr/Ta surface atomic ratio is considered to reflect differences in the distribution of each element in the respective samples. On the basis of results above, it appears that zirconium and tantalum atoms are mixed atomically in the solid solution, suggesting that the *m*-ZrO_2 components are segregated to the surface in the present *m*-ZrO_2/TaON sample. This is supported by the characterization results. As the Zr/Ta molar ratio employed in preparation increases from 0.1 (Entry 3) to 0.2 (Entry 4), both the Zr/Ta atomic ratio and O/Ta atomic ratio in the composite material increase, indicating that the introduced *m*-ZrO_2 is stacked on the TaON surface rather than mixed into the TaON crystal lattice. This is in good agreement with the results of XRD measurements, which indicate that the diffraction peaks assigned to *m*-ZrO_2 strengthen with increasing Zr/Ta molar ratio (Figure 3). On the other hand, the N/Ta surface atomic ratio in TaON did not change noticeably upon modification with *m*-ZrO_2 or formation of the solid solution with *m*-ZrO_2.

SEM images of the nitrided *m*-ZrO_2/Ta_2O_5 composite samples are shown in Figure 7. As reported previously, as-prepared TaON (Zr/Ta = 0) consists of primary particles of 300–500 nm in size with some pores (20–30 nm) and a relatively smooth surface.[16] The zirconium-containing samples, on the other hand, exhibit a rough surface morphology with no significant change in particle size with respect to the original TaON. The morphology becomes rougher with increasing Zr/Ta molar ratio, and for the sample prepared with the highest Zr/Ta ratio of 0.2, large aggregates of 50–100 nm in size are apparent. Considering the results of the XRD, XAFS, and XPS analyses, most of the introduced *m*-ZrO_2 is expected to be located on the surface of the TaON particles rather than in the bulk. Therefore, the observed morphology-roughening is considered to result from the introduction of *m*-ZrO_2. The specific surface area of the samples increases successively from 4.4 to 5.3 $m^2\,g^{-1}$ with increasing Zr/Ta molar ratio (from 0 to 0.2), consistent with the SEM observations. Previous investigations by high-resolution transmission electron microscopy (HR-TEM) revealed that the solid-state transformation of Ta_2O_5 to TaON by reaction with NH_3 is pseudomorphic and topotactic, producing single-crystalline particles of TaON with a porous structure from the particulate single-crystalline Ta_2O_5 precursor.[16] Therefore, the loading of nanoparticulate *m*-ZrO_2 onto Ta_2O_5 particles appears to have little effect on the nitridation mechanism from Ta_2O_5 to TaON despite modification of the surface structure.

Optical Properties of Nitridation Products. The UV–visible diffuse reflectance spectra for the same set of samples are shown in Figure 8. The absorption band edge of TaON (Zr/Ta = 0) appears at ca. 520 nm and is due to electron transition from the valence band formed by the hybridization of N 2p and O 2p orbitals to the conduction band consisting of empty Ta 5d orbitals.[2a,10,39] The increase in the background level (longer than 500 nm) of the TaON spectrum is attributable to the presence of reduced tantalum species (e.g., Ta^{3+}), which suggests the presence of surface defects that can act as recombination centers for photogenerated carriers. TaON is synthesized by the nitridation of Ta_2O_5 powder at 1123 K under NH_3 flow. At such high temperatures, the reductive atmosphere of nitridation can be expected to cause a fraction of the Ta^{5+} ion population on the surface of the TaON to be reduced. Similar behavior has been observed for other oxynitride-type materials, such as $LaTiO_2N$[29] and $TiN_xO_yF_z$,[30] which are nitrided in a similar manner to the present method. *m*-ZrO_2/TaON composites with Zr/Ta ratios of 0.05–0.2 exhibit similar absorption profiles to that of TaON, and the position of the absorption edge is largely unchanged from that of TaON. Guenther and Jansen reported that the absorption edge position of the *m*-ZrO_2–TaON solid solution is successively shifted to lower wavelengths with increasing *m*-ZrO_2 content.[28] As the present materials are not solid solutions but composites of *m*-ZrO_2 and TaON, the interaction between *m*-ZrO_2 and TaON is expected to be too weak to shift the absorption

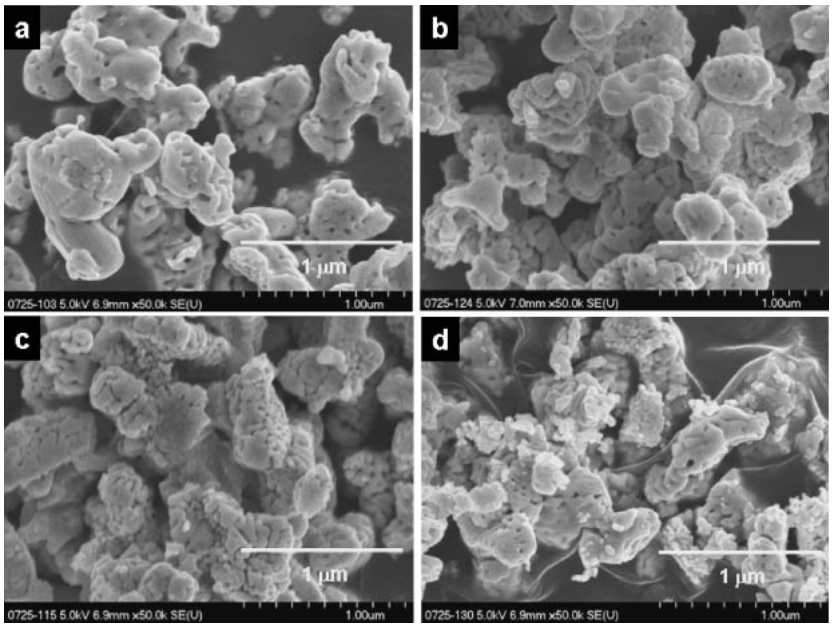

Figure 7. SEM images of samples obtained by nitriding m-ZrO_2/Ta_2O_5 with Zr/Ta molar ratios of (a) 0, (b) 0.05, (c) 0.1, and (d) 0.2 at 1123 K for 15 h under NH_3 flow.

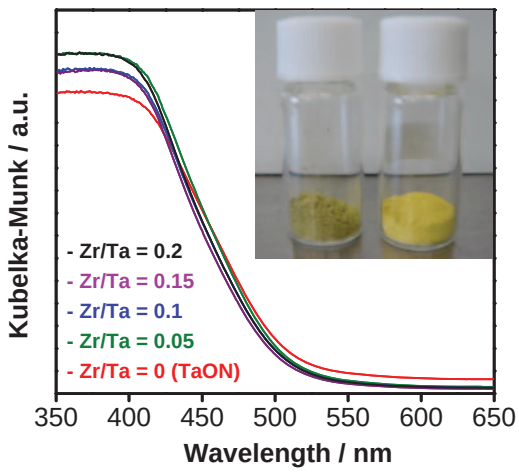

Figure 8. UV–visible diffuse reflectance spectra for samples obtained by nitriding m-ZrO_2/Ta_2O_5 with various Zr/Ta molar ratios at 1123 K for 15 h under NH_3 flow. (Inset) Photograph of samples with Zr/Ta molar ratios of 0 (left) and 0.1 (right).

edge of TaON to shorter wavelengths. However, minor structural mixing of m-ZrO_2 with TaON can be expected at the interface since m-ZrO_2 and TaON possess the same monoclinic baddelyite structure.[27,28]

An important observation to mention here is the decrease in the background level of TaON upon modification with m-ZrO_2, which indicates that m-ZrO_2 modification is effective for suppressing the formation of reduced tantalum species during nitridation. As mentioned above, the reduced tantalum species are considered to be generated near the surface of the TaON rather than in the bulk. Nitridation of the m-ZrO_2/Ta_2O_5 composite at 1123 K causes Ta_2O_5 to transform to TaON while preserving the original particle size as pseudomorphic and topotactic process.[16] The m-ZrO_2 itself does not undergo nitridation. Tantalum cations at the interface between Ta_2O_5 (and/or TaON) and the loaded m-ZrO_2 are expected to interact with m-ZrO_2 and thereby become more cationic. As a result, the formation of reduced tantalum species, which can act as recombination centers between photogenerated electrons and holes, on the TaON surface would be suppressed by prior loading with nanoparticulate m-ZrO_2. Whereas the formation of a solid solution between m-ZrO_2 and TaON results in a blue-shift of the absorption edge of TaON,[28] the formation of a composite of m-ZrO_2 and TaON allows the original absorption edge position of TaON (ca. 520 nm) to be maintained. This is desirable from the viewpoint of visible-light utilization in photocatalysis. The as-prepared TaON powder is yellowish-green in color, while the m-ZrO_2/TaON composite is brilliant yellow (Figure 8, inset). The above-mentioned idea that the reduction of tantalum species in the TaON surface during nitridation can be suppressed by modification with m-ZrO_2 seems to contradict the result of XPS analysis, which showed that the Ta $4f_{7/2}$ peak of the composite sample appeared at the same position as that of TaON (Figure 6). Presumably, the change in the state of surface tantalum species between the two samples is too small to detect by XPS measurement.

On the basis of the characterization above, it is concluded that the nitrided m-ZrO_2/Ta_2O_5 composites are not solid solutions of m-ZrO_2 and TaON but rather composites of m-ZrO_2 and TaON with monoclinic baddelyite structure and relatively low surface defect density.

Water Reduction and Oxidation Activity of m-ZrO_2/TaON Composite Catalysts. Figure 9A shows the dependence of the initial rate of H_2 evolution from aqueous methanol solution by Ru-loaded m-ZrO_2/TaON catalysts under visible light ($\lambda > 420$ nm) on the Zr/Ta molar ratio employed in preparation of the material. Since the rate of H_2 evolution from aqueous methanol solution by TaON modified with Ru is much faster than those achieved using other noble metals such as Pt,[2c] we employed Ru as a cocatalyst for H_2 evolution by

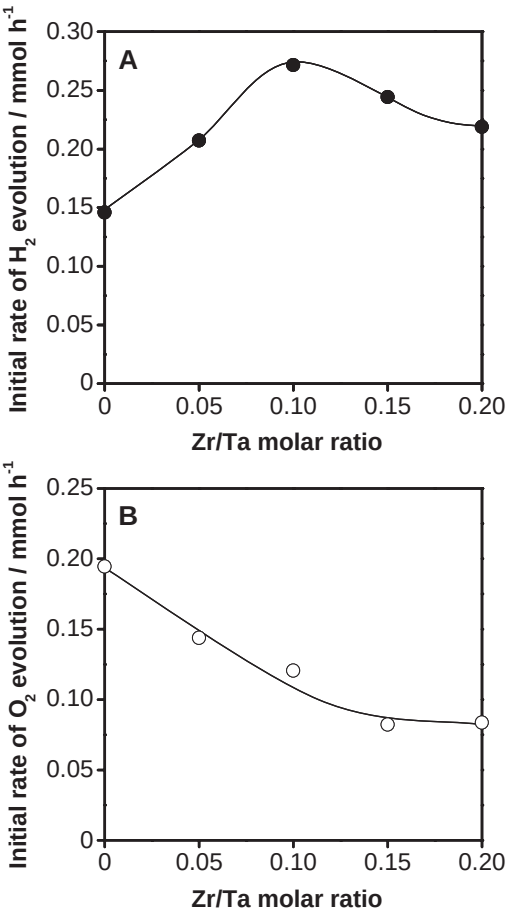

Figure 9. Dependence of initial rate of (A) H_2 evolution from an aqueous methanol solution (80 vol %) by Ru-loaded m-ZrO_2/TaON and (B) O_2 evolution from a silver nitrate solution (10 mM) containing 0.2 g of La_2O_3 by m-ZrO_2/TaON under visible light ($\lambda > 420$ nm) on Zr/Ta molar ratio of m-ZrO_2/TaON composite. Reaction conditions: catalyst, 0.4 g; reactant solution, 100 mL; light source, xenon lamp (300 W) with cutoff filter; reaction vessel, top inner-irradiation type.

the present photocatalysts to produce more H_2, thereby making it clear to judge the optimal Zr/Ta molar ratio. All catalysts produced H_2 upon irradiation at visible wavelengths. The rate of H_2 evolution increased with the Zr/Ta molar ratio to a maximum at Zr/Ta = 0.1, beyond which the activity of the catalysts began to decrease gradually.

The initial rate of O_2 evolution from aqueous silver nitrate solution under visible light is shown as a function of the Zr/Ta molar ratio in Figure 9B. In contrast to the case for H_2 evolution activity, the O_2 evolution activity decreased gradually with increasing Zr/Ta molar ratio, indicating that modification of the TaON surface with m-ZrO_2 has a detrimental effect on water oxidation.

The present m-ZrO_2/TaON catalyst is considered to undergo the following processes when exposed to visible light ($\lambda > 420$ nm). The TaON component absorbs photon energy greater than the band gap energy, generating electrons and holes in the conduction and valence bands, respectively. The conduction band electrons and valence band holes cause surface chemical reactions. However, the m-ZrO_2 component does not absorb photons at visible wavelengths because the band gap (ca. 5.0 eV) is too large to allow the absorption of visible light. No gas evolution was detected over m-ZrO_2 when employed as a photocatalyst under the present reaction conditions. Furthermore, as the bottom of the conduction band (−1.0 V, vs. NHE at pH 0) and the top of the valence band (+4.0 V, vs. NHE at pH 0)[23b] of m-ZrO_2 are more negative and more positive than those of TaON (conduction band edge, −0.3 V; valence band edge, +2.2 V),[7] respectively, electron transfer from the conduction band of TaON to the conduction band of m-ZrO_2 and transfer of holes from the valence band of TaON to the valence band of m-ZrO_2 should be energetically unfavorable. Based on such a scenario, m-ZrO_2 on the TaON surface will not take part in the charge-transfer process, even though m-ZrO_2 has been reported to function as a photocatalyst for methanol oxidation.[26] It is thus reasonable to conclude that under visible light, surface chemical reactions take place on the surface of the TaON component in the m-ZrO_2/TaON composite catalyst.

The introduction of m-ZrO_2 onto the surface of TaON appears to have at least two effects on activity; the positive effect of the suppression of surface defect formation (see Figure 8) related to the reduction of tantalum species under nitridation, and the negative effect of obscuring catalytically active sites on the TaON surface and thereby preventing TaON from participating in chemical reactions. In the case of H_2 evolution (Figure 9A), the increase in activity with increasing Zr/Ta molar ratio is attributable to the suppression of defect generation during nitridation. On the other hand, the reduction in activity over the compositional range of Zr/Ta = 0.1–0.2 can be ascribed to excess m-ZrO_2 coverage on the TaON surface. Nevertheless, the m-ZrO_2/TaON composite catalyst with Zr/Ta molar ratio of up to 0.2 exhibits higher activity than TaON alone. It thus appears that m-ZrO_2 has no detrimental effect on activity at compositions up to Zr/Ta = 0.2. In the case of O_2 evolution (Figure 9B), on the other hand, the negative effect of the m-ZrO_2 component on activity is significant, effectively overwhelming any increase in activity due to the positive effect (reduction of surface defects).

Nakamura et al. reported that TaON has similar oxidation ability for both water and methanol.[5] It is therefore speculated that the methanol oxidation ability of the m-ZrO_2/TaON catalyst will also be lower than that of TaON. If the oxidation ability of TaON for methanol oxidation by valence band holes is reduced upon modification with m-ZrO_2, water reduction by conduction band electrons should also be hindered due to the inefficient consumption of photogenerated holes. However, as seen here, the activity of the present catalyst for water reduction is higher than that for TaON (Figure 9A). The positive effect of m-ZrO_2 modification on water reduction activity may therefore be quite large, suggesting that the surface modification of TaON with m-ZrO_2 is an effective approach for enhancing the H_2 evolution activity of TaON. Although thermal reduction of metal cations in (oxy)nitrides during nitridation is one of the serious problems in (oxy)nitride-based photocatalysis, the present strategy that a nitridation-stable material is employed as a "protector" may be useful for other (oxy)nitride photocatalysts to improve activity.

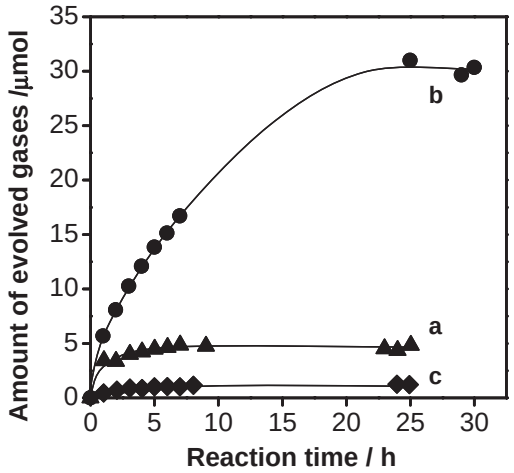

Figure 10. Time courses of H_2 evolution from aqueous NaI solution using (a) Pt-loaded TaON, (b) Pt-loaded *m*-ZrO_2/TaON (Zr/Ta = 0.1), and (c) Pt-loaded *m*-ZrO_2/TaON (Zr/Ta = 0.1) with the intentional addition of $NaIO_3$ (1 mM) under visible light ($\lambda > 420$ nm). Reaction conditions: catalyst, 0.1 g; cocatalyst, 0.5 wt % Pt; reactant solution, aqueous NaI solution (1 mM, 100 mL); light source, xenon lamp (300 W) with cutoff filter; reaction vessel, top inner-irradiation type.

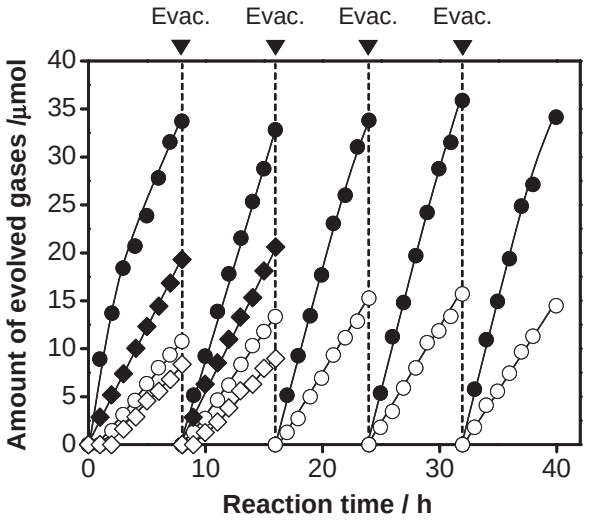

Figure 11. Time course of H_2 and O_2 evolution using a mixture of Pt-loaded *m*-ZrO_2/TaON and Pt-loaded WO_3 from aqueous NaI solution under visible light ($\lambda > 420$ nm). Data for the corresponding TaON-based system are also shown. Reaction conditions: catalyst, 0.2 g of each; cocatalyst, 0.5 wt % Pt; reactant solution, aqueous NaI solution (1 mM, 100 mL); light source, xenon lamp (300 W) with cutoff filter; reaction vessel, top inner-irradiation type. Solid circles, H_2 (*m*-ZrO_2/TaON-based system); open circles, O_2 (*m*-ZrO_2/TaON-based system); solid squares, H_2 (TaON-based system); open squares, O_2 (TaON-based system).

Application to Z-Scheme Overall Water-Splitting System. Our group has previously reported that the stoichiometric decomposition of pure water into H_2 and O_2 can be achieved under visible light ($\lambda > 420$ nm) using Pt-loaded TaON for H_2 evolution and Pt-loaded WO_3 for O_2 evolution in an IO_3^-/I^- shuttle redox-mediated system (Z-scheme overall water splitting).[4] The enhanced water reduction activity of the *m*-ZrO_2/TaON catalyst, as presented in the previous section, is also expected to be observed in the Z-scheme system. The most active of the *m*-ZrO_2/TaON composites (Zr/Ta = 0.1 by mole) was thus examined in combination with Pt-loaded WO_3 for the decomposition of pure water under visible light ($\lambda > 420$ nm). In this system, *m*-ZrO_2/TaON is the H_2 evolution catalyst, and Pt-loaded WO_3 is the O_2 evolution catalyst and IO_3^-/I^- shuttle redox mediator. Photocatalytic H_2 evolution was first examined using aqueous NaI solution. As reported previously, under visible light, Pt-loaded TaON produces H_2 from an aqueous solution containing NaI as an electron donor.[4] Visible-light-driven H_2 evolution was also observed using Pt-loaded *m*-ZrO_2/TaON (Zr/Ta = 0.1), as shown in Figure 10 (curve b). The initial activity of the Pt-loaded *m*-ZrO_2/TaON catalyst is approximately 1.6 times higher than that achieved using Pt-loaded TaON. However, the rate of H_2 evolution using either catalyst decreases as the reaction proceeds. This deactivation is ascribed to the backward reaction (photoreduction of IO_3^- by photogenerated electrons), which takes place in the conduction band of the catalyst.[4] When I^- is used as an electron donor for H_2 evolution with Pt-loaded TaON, IO_3^- is produced by the photooxidation of I^- by valence band holes. As IO_3^- is more susceptive to reduction than H^+ (IO_3^-/I^-, +0.67 V; H^+/H_2, −0.41 V vs. NHE at pH 7), H_2 evolution ceases when the concentration of IO_3^- reaches a certain level.[4,34] When the reaction was carried out in the presence of both I^- and IO_3^- (1 mM of each), the rate of H_2 evolution decreased markedly (Figure 10, curve c), providing evidence for the above competitive model. Similar behavior has been observed for Pt-loaded anatase-TiO_2 and Pt-loaded $SrTiO_3$ codoped with chromium and tantalum in H_2 evolution from aqueous NaI solution.[33,34] Compared with TaON, however, the *m*-ZrO_2/TaON (Zr/Ta = 0.1) composite is relatively robust with respect to the deactivation observed in the above reaction. This result implies that the selectivity of H^+ photoreduction by Pt-loaded *m*-ZrO_2/TaON (Zr/Ta = 0.1) is better than that by Pt-loaded TaON. In contrast, no O_2 evolution was observed when the Pt-loaded *m*-ZrO_2/TaON (Zr/Ta = 0.1) catalyst was irradiated with visible light in the presence of IO_3^- (10 mM), suggesting that I^- produced by the photoreduction of IO_3^- readily reacts with photogenerated holes in the valence band of the material.[4] These reactivities are desirable for H_2 evolution in Z-scheme overall water splitting using an IO_3^-/I^- shuttle redox mediator.[34]

Finally, Pt-loaded WO_3 as a catalyst for O_2 evolution was added to the aqueous solution containing Pt-loaded *m*-ZrO_2/TaON (Zr/Ta = 0.1) and NaI. A typical time course of H_2 and O_2 evolution under visible light is shown in Figure 11. Data for the TaON-based system is also shown for comparison. The gas phase was evacuated every 8 h, and the reaction was allowed to proceed for a total of 40 h to evaluate stability. In the initial stage of the reaction, the rate of O_2 evolution is slightly lower than that expected from the stoichiometry. As the reaction proceeds, however, the H_2/O_2 evolution ratio becomes close to the stoichiometric value ($H_2/O_2 = 2$). Clearly,

the *m*-ZrO_2/TaON-based catalytic system exhibits stable gas evolution behavior, and achieves better performance than the comparable TaON-based system. The total production of H_2 and O_2 after 40 h was 240 μmol, substantially larger than the total amount of NaI employed as a shuttle redox mediator (100 μmol). The simultaneous evolution of H_2 and O_2 was not observed when one component of the system (Pt-loaded *m*-ZrO_2/TaON (Zr/Ta = 0.1), Pt-loaded WO_3, NaI) was absent. In addition, no gas evolution was observed without irradiation. These results clearly demonstrate that overall water splitting proceeds photocatalytically according to the Z-scheme. However, it appears that the activity realized in the *m*-ZrO_2/TaON system is only approximately 1.5 times higher than that achieved using TaON, despite the promising catalytic performance of Pt-loaded *m*-ZrO_2/TaON in H_2 evolution from aqueous NaI solution (Figure 10). It has been reported that IO_3^- anions in the solution, even at low concentrations, readily adsorb onto the surface of Pt-loaded WO_3, efficiently reacting with photogenerated electrons in the catalyst and thereby achieving efficient O_2 evolution.[34] The prompt photoreduction of IO_3^- to I^- on Pt-loaded WO_3 ensures that the concentration of IO_3^- in the reactant solution remains very low during the reaction,[4] effectively suppressing the photoreduction of IO_3^- to I^- (undesirable backward reaction) on the H_2 evolution photocatalyst. As a result, the enhanced catalytic performance of Pt-loaded *m*-ZrO_2/TaON for H_2 evolution from aqueous NaI solution may be obscured under the Z-scheme conditions by the strong activity of Pt-loaded WO_3 for the reduction of IO_3^- to I^-. Nevertheless, the higher activity of the *m*-ZrO_2/TaON-based system compared to the TaON-based system can be reasonably attributed to the enhanced activity for water reduction resulting from the lower density of surface defects, although the quantum efficiency of both systems are almost comparable. The enhancement of water reduction activity is considered critical to developing a highly efficient Z-scheme overall water-splitting system consisting of Pt-loaded WO_3 as an O_2 evolution catalyst and an IO_3^-/I^- shuttle redox mediator. Further improvement of the activity of this system, including refinement of the catalyst preparation method and reaction conditions, will be published as part of future work.

Conclusion

A composite material consisting of *m*-ZrO_2 and TaON (Zr/Ta = 0–0.2 by mole) was successfully prepared by nitriding Ta_2O_5 loaded with nanoparticulate *m*-ZrO_2 at 1123 K for 15 h under NH_3 flow. When loaded with appropriate noble metals to promote H_2 evolution, the composite material is active for the photocatalysis of H_2 evolution from aqueous methanol solution and Z-scheme overall water splitting, achieving higher activity than for TaON alone. Suppression of the generation of reduced tantalum species during nitridation is shown to be important to enhance H_2 evolution activity of TaON.

This work was supported by the Research and Development in a New Interdisciplinary Field Based on Nanotechnology and Materials Science program of the Ministry of Education, Culture, Sports, Science and Technology (MEXT) of Japan. Acknowledgement is extended to Tokyo Metropolitan Industrial Technology Research Institute for financial support. One of the authors (K.M.) gratefully acknowledges the support of a Japan Society for the Promotion of Science (JSPS) Fellowship.

Supporting Information

XRD patterns of samples obtained by solid-state reaction between $ZrO(NO_3)_2 \cdot 2H_2O$ and Ta_2O_5 in air at 1073 K for 2 h with different Zr/Ta molar ratios (Figure S1) and Ta–L_I edge XANES spectra for samples obtained by nitriding *m*-ZrO_2/Ta_2O_5 with different Zr/Ta molar ratios at 1123 K for 15 h under NH_3 flow. This material is available free charge on the Web at: http://www.csj.jp/journals/bcsj/.

References

1 From the viewpoint of nomenclature, "tantalum oxynitride (TaON)" should be presented as "tantalum nitride oxide (TaNO)." In this paper, "TaNO" is expressed as "TaON" for convenience, because the term "TaON" has been accepted in many published papers relevant to the material (see Refs. 2–10, 16, and 39).

2 a) G. Hitoki, T. Takata, J. N. Kondo, M. Hara, H. Kobayashi, K. Domen, *Chem. Commun.* **2002**, 1698. b) M. Hara, G. Hitoki, T. Takata, J. N. Kondo, H. Kobayashi, K. Domen, *Catal. Today* **2003**, *78*, 555. c) M. Hara, J. Nunoshige, T. Takata, J. N. Kondo, K. Domen, *Chem. Commun.* **2003**, 3000. d) M. Hara, T. Takata, J. N. Kondo, K. Domen, *Catal. Today* **2004**, *90*, 313.

3 S. Ito, K. R. Thampi, P. Comte, P. Liska, M. Grätzel, *Chem. Commun.* **2005**, 268.

4 R. Abe, T. Takata, H. Sugihara, K. Domen, *Chem. Commun.* **2005**, 3829.

5 R. Nakamura, T. Tanaka, Y. Nakato, *J. Phys. Chem. B* **2005**, *109*, 8920.

6 R. Abe, T. Takata, H. Sugihara, K. Domen, *Chem. Lett.* **2005**, *34*, 1162.

7 W. A. Chun, A. Ishikawa, H. Fujisawa, T. Takata, J. N. Kondo, M. Hara, M. Kawai, Y. Matsumoto, K. Domen, *J. Phys. Chem. B* **2003**, *107*, 1798.

8 M. Hara, E. Chiba, A. Ishikawa, T. Takata, J. N. Kondo, K. Domen, *J. Phys. Chem. B* **2003**, *107*, 13441.

9 K. Maeda, K. Domen, *J. Phys. Chem. C* **2007**, *111*, 7851.

10 M. Yashima, Y. Lee, K. Domen, *Chem. Mater.* **2007**, *19*, 588.

11 A. Kudo, A. Tanaka, K. Domen, T. Onishi, *J. Catal.* **1988**, *111*, 296.

12 S. Ikeda, M. Hara, J. N. Kondo, K. Domen, H. Takahashi, T. Okubo, M. Kakihana, *Chem. Mater.* **1998**, *10*, 72.

13 J. Sato, H. Kobayashi, K. Ikarashi, N. Saito, H. Nishiyama, Y. Inoue, *J. Phys. Chem. B* **2004**, *108*, 4369.

14 K. Maeda, K. Teramura, T. Takata, M. Hara, N. Saito, K. Toda, Y. Inoue, H. Kobayashi, K. Domen, *J. Phys. Chem. B* **2005**, *109*, 20504.

15 K. Maeda, N. Saito, Y. Inoue, K. Domen, *Chem. Mater.* **2007**, *19*, 4092.

16 D. Lu, G. Hitoki, E. Katou, J. N. Kondo, M. Hara, K. Domen, *Chem. Mater.* **2004**, *16*, 1603.

17 K. Sayama, H. Arakawa, K. Domen, *Catal. Today* **1996**, *28*, 175.

18 a) H. Kominami, S. Murakami, Y. Kera, B. Ohtani, *Catal. Lett.* **1998**, *56*, 125. b) H. Kominami, S. Murakami, J. Kato, Y. Kera, B. Ohtani, *J. Phys. Chem. B* **2002**, *106*, 10501.

19 B. C. H. Steele, A. Heinzel, *Nature* **2001**, *414*, 345.

20 R. Stevens, *An Introduction to Zirconia and Zirconia*

Ceramics, 2nd ed., Magnesium Elektron Ltd., Twikenham, UK, **1986**.

21 a) T. Yamaguchi, *Catal. Today* **1994**, *20*, 199. b) G. D. Yadav, J. J. Nair, *Microporous Mesoporous Mater.* **1999**, *33*, 1.

22 K. M. Ganguly, S. Sarkar, S. N. Bhattacharyya, *J. Chem. Soc., Chem. Commun.* **1993**, 682.

23 a) K. Sayama, H. Arakawa, *J. Phys. Chem.* **1993**, *97*, 531. b) K. Sayama, H. Arakawa, *J. Photochem. Photobiol., A* **1994**, *77*, 243.

24 Y. Kohno, T. Tanaka, T. Funabiki, S. Yoshida, *J. Chem. Soc., Faraday Trans.* **1998**, *94*, 1875.

25 a) S. G. Botta, J. A. Navío, M. C. Hidalgo, G. M. Restrepo, M. I. Litter, *J. Photochem. Photobiol., A* **1999**, *129*, 89. b) J. A. Navío, M. C. Hidalgo, G. Colón, S. G. Botta, M. I. Litter, *Langmuir* **2001**, *17*, 202.

26 C. Wu, X. Zhao, Y. Ren, Y. Yue, W. Hua, Y. Cao, Y. Tang, Z. Gao, *J. Mol. Catal. A: Chem.* **2005**, *229*, 233.

27 J. Grins, P.-O. Käll, G. Svensson, *J. Mater. Chem.* **1994**, *4*, 1293.

28 E. Guenther, M. Jansen, *Mater. Res. Bull.* **2001**, *36*, 1399.

29 a) A. Kasahara, K. Nukumizu, G. Hitoki, T. Takata, J. N. Kondo, M. Hara, H. Kobayashi, K. Domen, *J. Phys. Chem. A* **2002**, *106*, 6750. b) A. Kasahara, K. Nukumizu, T. Takata, J. N. Kondo, M. Hara, H. Kobayashi, K. Domen, *J. Phys. Chem. B* **2003**, *107*, 791.

30 a) K. Nukumizu, J. Nunoshige, T. Takata, J. N. Kondo, M. Hara, H. Kobayashi, K. Domen, *Chem. Lett.* **2003**, *32*, 196. b) K. Maeda, Y. Shimodaira, B. Lee, K. Teramura, D. Lu, H. Kobayashi, K. Domen, *J. Phys. Chem. C* **2007**, *111*, 18264.

31 T. Mishima, M. Matsuda, M. Miyake, *Appl. Catal., A* **2007**, *324*, 77.

32 M. Kakihana, M. M. Milanova, M. Arima, T. Okubo, M. Yashima, M. Yoshimura, *J. Am. Ceram. Soc.* **1996**, *79*, 1673.

33 K. Sayama, K. Mukasa, R. Abe, Y. Abe, H. Arakawa, *J. Photochem. Photobiol., A* **2002**, *148*, 71.

34 R. Abe, K. Sayama, H. Sugihara, *J. Phys. Chem. B* **2005**, *109*, 16052.

35 S. Inoue, H. Oki, Z. Hagiwara, *J. Inorg. Nucl. Chem.* **1975**, *37*, 929.

36 B. Samaranch, P. R. de la Piscina, G. Clet, M. Houalla, P. Gelin, N. Homs, *Chem. Mater.* **2007**, *19*, 1445.

37 JCPDF No. 37-1484.

38 a) S. Ardizzone, M. G. Cattania, P. Lugo, *Electrochim. Acta* **1994**, *39*, 1509. b) S. Ardizzone, C. L. Bianchi, *Surf. Interface Anal.* **2000**, *30*, 77.

39 C. M. Fang, E. Orhan, G. A. Wijs, H. T. Hintzen, R. A. Groot, R. Marchand, J. Y. Saillard, G. With, *J. Mater. Chem.* **2001**, *11*, 1248.